Hydrogen Storage in Graphene-Based Materials

Spyrou, Konstantinos; Gournis, Dimitrios; Rudolf, Petra

Published in:
ECS Journal of Solid State Science and Technology

DOI:
10.1149/2.018310jss

Publication date:
2013

ECS Journal of Solid State Science and Technology, **2** (10) M3160-M3169 (2013)
2162-8769/2013/2(10)/M3160/10/$31.00 © The Electrochemical Society

JSS Focus Issue on Nanocarbons for Energy Harvesting and Storage

Hydrogen Storage in Graphene-Based Materials: Efforts Towards Enhanced Hydrogen Absorption

Konstantinos Spyrou,[a] Dimitrios Gournis,[b] and Petra Rudolf[a,z]

[a]*Zernike Institute for Advanced Materials, University of Groningen, NL-9747AG Groningen, The Netherlands*
[b]*Department of Materials Science and Engineering, University of Ioannina, GR-45110 Ioannina, Greece*

The discovery in 2004 that graphene can be produced by micromechanical exfoliation brought forth a plethora of unique electronic, mechanical, thermal and optical properties of this first stable two dimensional (2-D) material ever isolated, which afforded the Nobel Prize to Andrei Geim and Konstantin Novoselov in 2010. One of the peculiarities of graphene is its extremely high specific surface area, which in combination with its low weight, robustness and chemical inertness places it among the most suitable materials for hydrogen storage devices. In this review we discuss the experimental and theoretical approaches applied so far to harness graphene and its derivatives as main building blocks for hydrogen uptake and storage; the potential of each approach for future applications in the hydrogen economy will also be examined.
 [DOI: 10.1149/2.018310jss]

Manuscript submitted August 1, 2013; revised manuscript received September 9, 2013. Published September 25, 2013. *This paper is part of the JSS Focus Issue on Nanocarbons for Energy Harvesting and Storage.*

The ever-increasing worldwide demands for energy consumption, along with the shortage of non-renewable fossil fuels (petroleum, coal, oil, gas) has forced the scientific community to investigate alternative sustainable energy sources. In this context pollution and climate change induced by the combustion products of currently used fuels add urgency to this difficult effort of developing to environmentally clean fuels.

Hydrogen is a renewable, efficient and environmentally friendly energy source and has great potential to replace non-renewable hydrocarbons for mobility and transport applications, which account for approximately one third of the current energy consumption, and thereby reduce CO_2 production on earth since its unique combustion product is clean water.[1,2] Hydrogen is the ideal 'green' fuel also because it is lightweight, nontoxic, very simple in structure (one proton and one electron in its neutral form), and available in enormous amounts since it is the most abundant element in the universe.

However, the utilization of molecular hydrogen as energy carrier requires two basic steps to be accomplished, namely a) hydrogen production and b) hydrogen storage. Desirable isolated molecular hydrogen (H_2) exists in strikingly low amounts (less than 1%) on earth. Most of the hydrogen is present on our planet chemically bound in water (H_2O) but also found in compounds such as ammonia (NH_3), or hydrocarbons and also makes up a large part of the molecules composing living organisms. The most sustainable way to produce hydrogen exploits solar energy in photocatalytic reactions.[3] The second step of reversible hydrogen storage in appropriate materials or adsorbed on suitable surfaces still requires many issues to be solved before becoming economically viable for all envisioned applications.

Currently employed technologies concern the reversible process of solution of hydrogen in metallic alloys and metal hydride formation for example hybrid vehicles use electrochemical hydride formation for storage of electricity. However, metal alloys as hydrogen storage media suffer from very low reversibility (hydrogenation/dehydrogenation), are very heavy and extremely expensive for daily use. On the other hand compressed gas in cylinders at high pressures as well as cryogenic storage are both unsuitable and unsafe for routine mobility and transport purposes.[4]

Carbon materials such as activated carbons[5] metal organic frameworks,[6,7] carbon nanotubes,[8] graphite nanofibers[9] and other carbon nanostructures[10] are considered promising candidates in hydrogen storage technology because they have a number of remarkable properties such as high specific surface areas, tunable pore structure, low density, stability for large scale production and fast kinetics,[8,11,12,13] have been studied extensively for hydrogen storage. Despite the huge effort spent in studying carbon nanostructures for hydrogen storage, no candidate material could reach the U.S Department of Energy gravimetric and volumetric targets for hydrogen storage systems which were set to 6.0 wt% and 45 g H_2/L, respectively for 2010. The new targets set for 2015[14] of a hydrogen gravimetric capacity of 9.0 wt% and volumetric capacity of 81 g/L seem reachable from the theoretical point of view, as we shall show in this review but represent a huge challenge on the experimental side.

The big challenge for carbon nanoporous materials as hydrogen storage media is to find a structure with tunable porosity and very high specific surface area, where hydrogen adsorbs strongly enough on the surface as to form a thermodynamically stable arrangement but not too strongly so that reversible fast loading/unloading kinetics are possible.

In 2004 Geim and Novoselov added a new member to the family of carbon nanostructures, namely graphene,[15] the one atom thick layer of carbon atoms tightly packed into a hexagonal lattice and revealed many of the extraordinary properties of this first ever isolated two-dimensional (2-D) structure. Graphene is unique concerning its electronic,[16] mechanical,[17] thermal[18] and optical[19] properties. Its surface specific area, a decisive factor for hydrogen storage applications, is theoretically estimated[20] to amount to 2630 $m^2\ g^{-1}$ and therefore much higher than that of other carbon structures such as carbon nanotubes.[21] This places graphene at the top of the list of potential candidates as hydrogen storage media.

Graphene and Hydrogen Storage

Hydrogen can interact with graphene surfaces by physisorption or chemisorption. Physisorbed hydrogen presents very fast kinetics due to London forces but is thermodynamically not very stable because of the small binding energies with the graphene matrix. On the other hand, chemisorbed hydrogen can be stored very efficiently owing to the strong interactions with the graphene layers; in this case the reversibility of the adsorption process constitutes the bottleneck for designing an effective storage material. The energy level diagram drawn up by Tozzini and Pellegrini[22] and presented in Figure 1 illustrates well the issues at stake for storing both atomic and molecular hydrogen. In this review we report on both experimental and theoretical studies implemented to realize graphene-based materials with a high hydrogen storage capacity.

A full understanding of the H_2 adsorption mechanism on graphitic materials is crucial to improve their hydrogen storage capacity. For this reason plenty calculations have been applied to various carbon systems. In 2005, Patchkovskii et al.[23] addressed the question why the U.S. Department of Energy goals of 6.5% mass ratio and 62 kg/m^3

[z]E-mail: p.rudolf@rug.nl

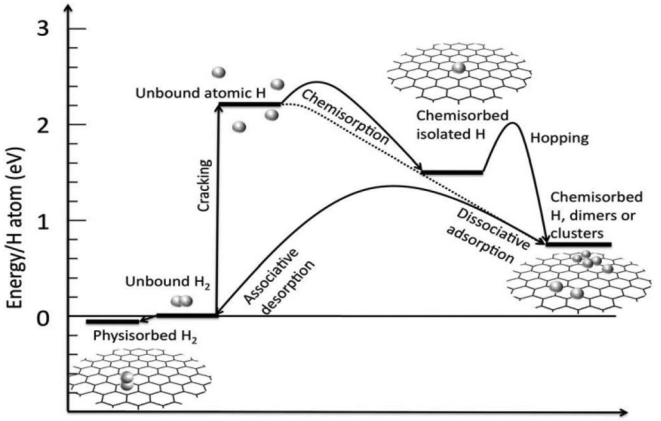

Figure 1. Energy level diagram for the graphene–hydrogen system. The energy is in eV per H atom, i.e. to obtain the values per H_2 each energy level and barrier value must be doubled. Values of energy levels are deduced both from experimental and theoretical evaluations; average values were taken when different values were available. Barriers are mainly derived from theoretical evaluations. The reference level is the pristine graphene plus unbound molecular hydrogen. [Reproduced with permission from Ref. 22].

volume density had not been achieved via theoretical simulations on reversible model systems.[24–27] They showed that insufficiently accurate carbon–H_2 interaction potentials, together with the neglect or the incomplete treatment of the quantum effects in previous theoretical investigations, led to misleading conclusions for the absorption capacity. By calculating the binding capacity for hydrogen at near ambient conditions including the quantum effects with ab initio interaction potentials, Patchkovskii et al.[23] pointed out that the low attractive H_2-graphene free reaction energy at 300 K makes graphite unsuitable for H_2 storage in practical circumstances. However, when the interlayer distance (*d*) of the graphene layers that compose graphite is increased, the physisorption free energy increases and hence also the binding energy for H_2 on graphene substrates, as shown in Table I for *d* values between 4 Å and 14 Å. An interlayer distance of approximately 6-7 Å was found to be optimal and theoretically capable of reaching a volumetric density complying with D.O.E targets (31 cm^3/mol) as illustrated in Figure 2.

A very original theoretical investigation by Tozzini and Pellegrini[28] showed that gravimetric capacities of up to 8% can be reached while at the same time achieving good reversibility for chemisorbed hydrogen on corrugated graphene sheets. The mechanism they propose for fast loading/uploading of hydrogen is depicted in Figure 3 and relies on release via the controlled inversion of the curvature of the graphene sheet. Two years later Goler et al.[29] by using Scanning Tunneling Microscopy (STM) techniques further have extended the investigations for adsorption and release of hydrogen atoms on monolayer graphene,

Table I. Free energy of H_2 adsorption on graphite surfaces and in graphite layered structures (Reproduced with permission from Ref. 23).

d, Å	ΔE_0, *Kj/mol	ΔF_{300}, Kj/mol	ΔE_{300}, Kj/mol	ΔS_{300}, J/mol-K	K_{300}
∞†	−6.2	−1.2	−2.4	−4.0	1.6
12.0	−6.4	−4.2	−5.3	−3.7	5.5
10.0	−6.7	−5.2	−6.0	−2.9	7.9
9.0	−7.1	−5.9	−6.7	−2.5	10.8
8.0	−8.1	−7.2	−8.1	−2.7	18.3
7.0	−11.0	−8.7	−10.8	−6.7	33.3
6.0‡	−13.0	−10.0	−13.1	−10.4	54.6
5.5‡	−10.1	−5.7	−10.1	−14.7	9.9
5.0‡	+1.2	+7.2	+1.7	−18.2	0.06

Results for quantum computations for ideal-gas H_2 in external graphite potentials. Parameter d is the interlayer distance. $\Delta F_0 = \Delta E_0$ and ΔF_{300} are free energies of H_2 adsorption at 0 K and 300 K, respectively. The energy and the entropy of adsorption at 300 K are given by ΔE_{300} and ΔS_{300}, and K_{300} is the equilibrium constant.
*H_2 ground state energy in the adsorbing potential.
†The infinite distance is computed in a box with interlayer spacing of d = 43Å.
‡Values at these interlayer separations may be affected by the shape of the repulsive part of the potential, leading to an increase in the error parts.

as a function of curvature of the atomic layers. These measurements confirmed that by controlling the local curvature of graphene layers, a promising material for hydrogen storage applications could be created.

Hydrogen Storage in Graphene Oxide (GO) and Reduced Graphene Oxide (rGO)

A material that has been recently studied for numerous applications is graphite oxide (GO), a derivative of graphite obtained by treatment with strong oxidants and easily exfoliated by rapid heating.[30] GO is potentially a good candidate also for hydrogen storage applications because it unites the advantages of graphene - high surface area, light weight, environmental friendliness and low processing cost - with the presence both on the surfaces and at the edges of the sheets of oxygen-containing functional groups that allow for further chemical modification, for example with transition metals. The latter can play a key role in hydrogen adsorption by providing the ideal binding strength with H_2, as reported by Wang et al.[31] who produced a storage material where Ti interacts with the hydroxyl groups of GO (450 kJ/mol) and is thus prevented from clustering, and number of hydroxyls on the surface of GO is tuned so that gravimetric and volumetric capacities of 4.9 wt% and 64 g/L, respectively can be achieved.

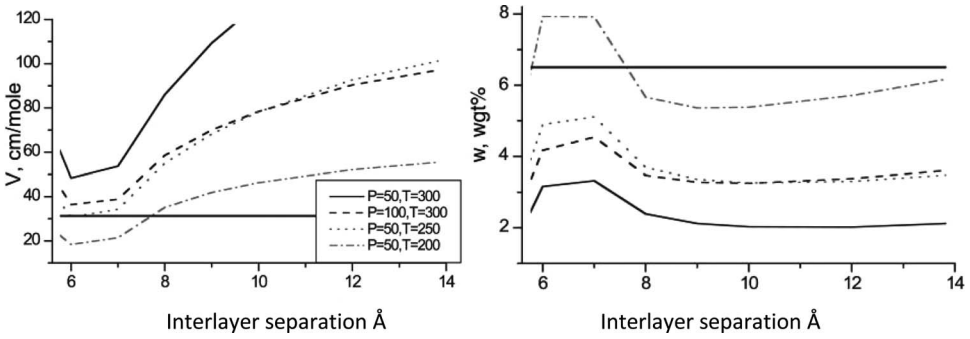

Figure 2. Gravimetric (*left*) and volumetric (*right*) H_2 storage capacities of layered graphite structures, calculated from the real gas equation of state, as functions of the interlayer separation. The DOE targets for automotive applications ($w = 6.5\%$, $v = 31.2$ cm^3/mol) are indicated by solid horizontal lines. [Reproduced with permission from Ref. 23].

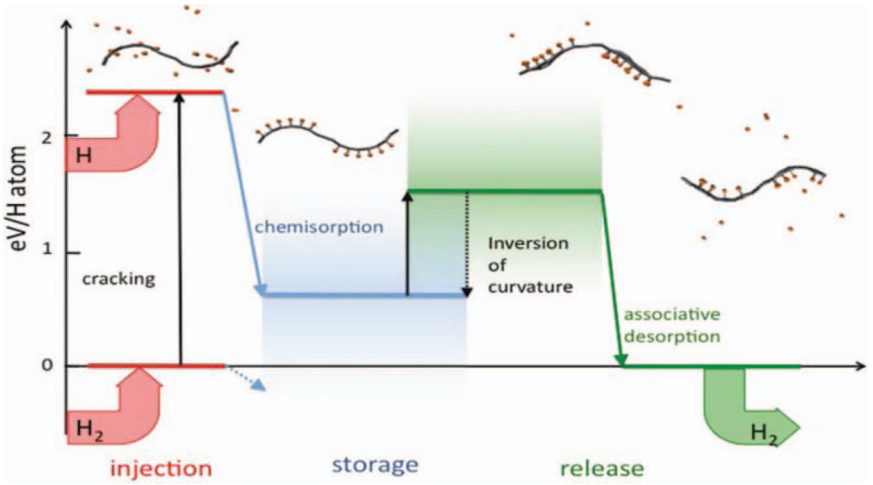

Figure 3. Working scheme of the microscopic mechanism for hydrogen storage proposed by Tozzini and Pellegrini[27]. Three phases can be distinguished: during the injection (red) the atomic hydrogen is cracked and introduced in the system. H chemisorbs on the convex regions during the storage phase (blue). The release phase (green) is activated by inversion of curvature, causing the associative desorption of H_2. The horizontal lines are placed according to the effective energies/H atom (shades represent range of energy variability). Representative snapshots are reported: the graphene sheet is represented in gray and the hydrogen in orange. [Reproduced with permission from Ref. 28].

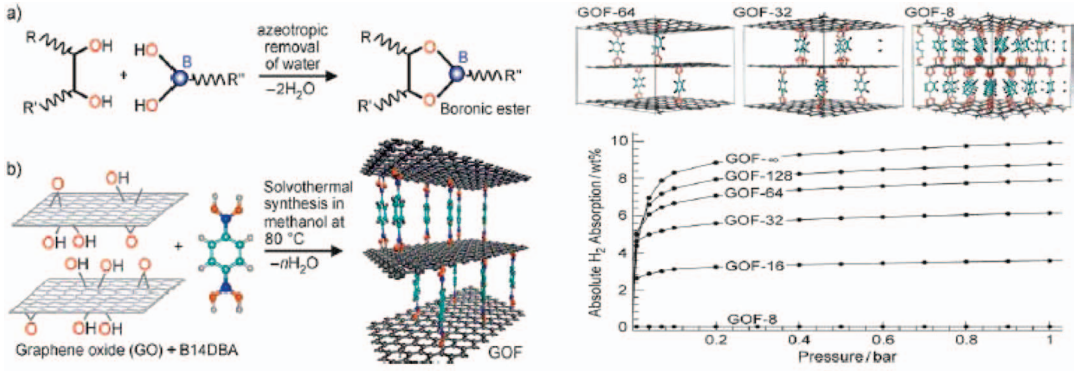

Figure 4. (left) Representations of a) boronic ester and b) GOF formation. Idealized graphene oxide framework (GOF) materials proposed in this study are formed of layers of graphene oxide connected by benzenediboronic acid pillars. (right) Grand canonical Monte Carlo simulations for ideal GOF-n structures with n graphene carbons per linker. The structures of three examples with n = 64, 32, and 8 are also shown. [Reproduced with permission from Ref. 32].

Alternatively the oxygen-containing groups can be further functionalized to increase the spacing between GO layers in a way which preserves enough the free surface on the GO layers for adsorption. Burress et al.[32] have linked boronic acid to GO to form new layered structures (Figure 4 left) called graphite organic frameworks (GOF). These authors theoretically predict competitive hydrogen adsorptions at 77 K (Figure 4 right) for GOFs with different linker densities.

A breakthrough for high hydrogen chemisorption on synthesized graphene oxide samples happened in 2010 when Subrahmanyam et al.[33] showed that graphene oxide samples could be reduced to hydrogenated few-layer graphene by means of a Birch reaction with lithium in liquid ammonia. Few layer graphene was prepared by exfoliation of graphite oxide[34] and hydrogenation of produced few-layer graphene by arc-evaporation techniques.[35] Graphite oxide and hydrogenated few-layer graphene suffered Birtch reduction with lithium in liquid ammonia.[36,37] With Brunauer-Emmet-Teller (BET) measurements the authors demonstrated that the samples exhibited high surface areas and elemental analysis showed storage capacities of 5 wt% under excess Li values, very promising for automotive applications. The energies of hydrogen interacting with the graphene surface at different sites and distances for different coverages were calculated and it was found that the binding energy of H atoms with graphene is largest for 50% coverage, corresponding to 4 wt%.[33]

Enhanced hydrogen storage by thermally exfoliated graphene derived from graphene oxide has been also reported by Jin et al.[38] The final material was obtained by extremely fast heating of graphite oxide under H_2/Ar gas flow and thereafter shortly annealed at 1000°C in the H_2/Ar gas flow in order to reduce the oxygen containing groups before functionalization as shown in Figure 5, to create the appropriate combination of interlayer space and available surface area on the reduced

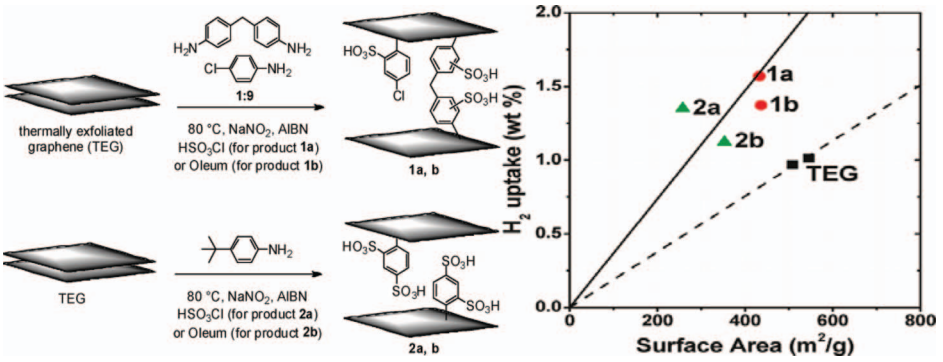

Figure 5. left panel: Functionalization and cross-linking of thermally exfoliated graphene sheets in chlorosulfonic acid and oleum. [Reproduced with permission from Ref. 36] right panel: Specific surface area determined from nitrogen BET at 77 K versus hydrogen uptake capacity at 77 K and 2 bar. The data of different materials are represented by different symbols: black squares, original thermally exfoliated graphene; red circles, products **1a** and **1b**; and green triangles, products **2a** and **2b**. The solid line is the fit and extrapolation from the data of functionalized thermally exfoliated graphene products. The dashed line correlates to the data of original thermally exfoliated graphene. [Reproduced with permission from Ref. 38].

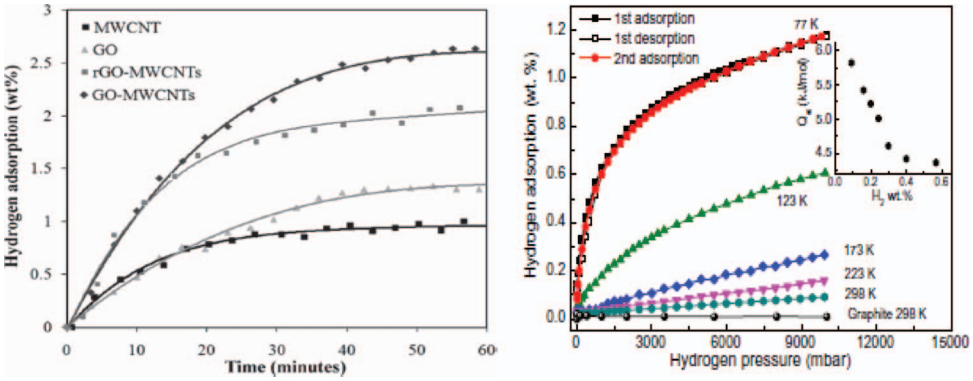

Figure 6. (left panel) Hydrogen adsorption of GO, multi-walled carbon nanotubes, and frameworks of GO and multi-walled carbon nanotubes and reduced GO and multi-walled carbon nanotubes as a function of time. (right panel) Hydrogen adsorption–desorption isotherms of graphene powder at various temperatures in the range of 77–298 K and pressures up to 10 bar. Inset: the isosteric heat of adsorption versus adsorption capacity. The hydrogen uptake isotherm of graphite powder (1–2 micron, synthetic from Aldrich) is measured at 298 K for comparison. [Reproduced with permission from Ref. 39 (left) and 40 (right)].

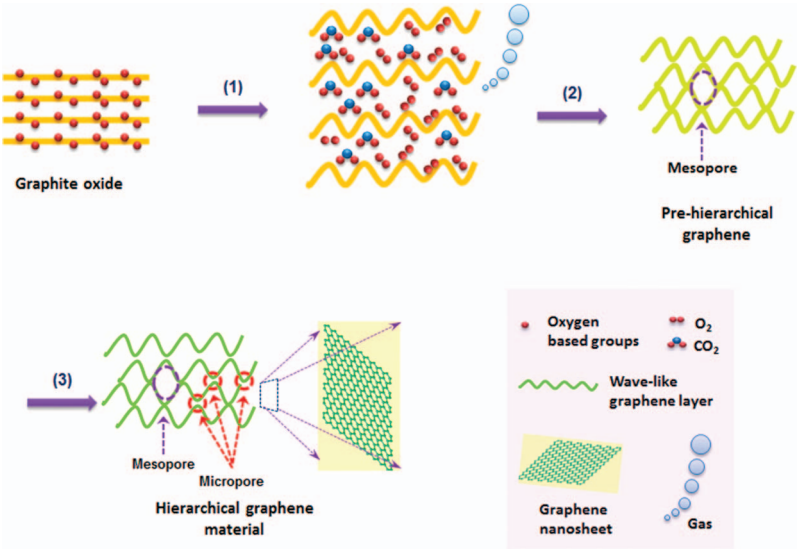

Figure 7. Scheme for the formation process of the hierarchical graphene-based material. [Reproduced with permission from Ref. 41].

graphene oxide sheets. The specific surface areas[38] determined from nitrogen BET measurements of these materials are shown in the right panel of Figure 5.

Other attempts with reduced graphite oxide[39] or graphene oxide frameworks intercalated with multi-walled carbon nanotubes[40] as 1-D spacers for hydrogen storage applications did not approach the D.O.E. requirements for automobile applications as illustrated in Figure 6.

Very recently Guo et al.[41] have succeeded to produce the highest experimental values for hydrogen adsorption by physisorption on graphene starting from graphite oxide by a procedure which is presented in Figure 7. They started out with graphene oxide which they heated in vacuum at low temperature (150°C) (steps 1 & 2) to induce an explosive-like exfoliation transforming it into a fluffy black powder, called by the authors "prehierarchical graphene material". This material was then treated at higher temperature (600°C) in Ar, resulting in a highly loose and black powder (step 3), which the authors describe as "hierarchical graphene-based material" because it contains micropores (0.8 nm), mesopores (4 nm) and macropores (>50 nm). Due to its very high specific area (1305 m^2 g^{-1}) more than 4wt% hydrogen can be adsorbed on this material approaching the 2010 D.O.E. targets (Figure 8). Guo and co-workers[41] have also suggested that these high

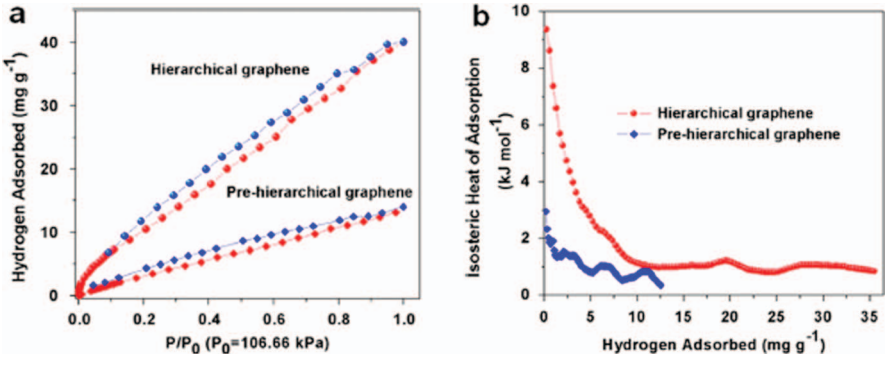

Figure 8. (a) Hydrogen adsorption and desorption isotherms of hierarchical graphene and prehierarchical graphene. (b) Isosteric heat of hydrogen sorption. [Reproduced with permission from Ref. 41].

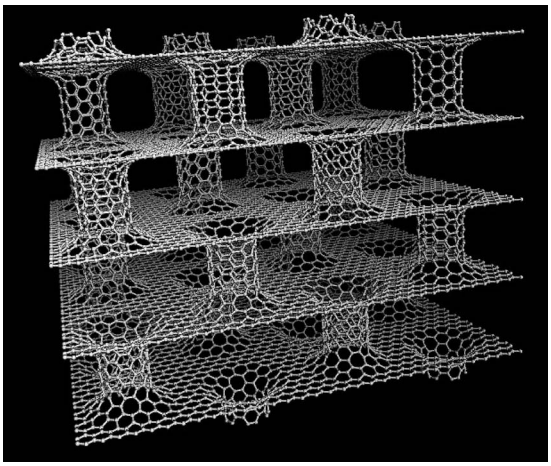

Figure 9. Pillared graphene. A novel 3-D network nanostructure proposed for enhanced hydrogen storage. [Reproduced with permission from Ref. 42].

values of hydrogen uptake might be significantly increased by metal doping, surface functionalization, and edge-site tailoring.

Hydrogen Storage in Pillared Graphene Structures

The pillaring method is a process by which a layered intercalated structure is converted into a thermally stable, mesoporous material with large surface area. A theoretical approach by the group of Froudakis[42] proposes a novel three dimensional (3-D) material[43] consisting of graphene layers connected by carbon nanotubes (CNTs) acting as 'pillars' (Figure 9), which stabilize the structure and keep the graphene layers at a fixed distance. Theoretical simulations[42] demonstrate that hydrogen interacts weakly with the carbon surface in such a structure and the gas uptake fluctuates at low values far from the D.O.E. gravimetric and volumetric targets, even at elevated temperatures and pressures (Figure 10). However, if Li-doping is introduced, the hydrogen uptake of these pillared graphene structures can be increased tremendously to reach values that almost approach the D.O.E. targets at ambient conditions (Figure 10).

The significant increase of hydrogen adsorption upon Li-doping of the pillared graphene led Froudakis and co-workers[44] to propose a new class of Li-doped materials based on graphene oxide. Functional hydroxyl (OH) groups of GO are substituted with Li atoms in order to form OLi functional groups, which have been demonstrated to increase the interaction of the material with H_2 due to dipole-induced dipole interactions of $-O^-Li^+$ and H_2.[45] These new materials have been predicted to be stable and to adsorb extremely high amounts of hydrogen reaching more than 10 wt% gravimetric capacity at 77 K and 100 bar (depending also on the carbon to oxygen ratio during the oxidation process and pore spacing) (Figure 11). Another interesting pillared structure has been suggested by Kuc et al.[46] as a candidate for fuel cells. Their theoretical investigation focussing on a recently synthesized graphene pillared with C_{60} molecules (Figure 12 left),[47] has confirmed the structural stability of this hybrid and proven that by reducing the amount of C_{60} in between the graphene layers the H_2 loading can be tuned to very competitive levels (Figure 12 right).

The first experimental effort on hydrogen storage in pillaring graphene by Matsuo et al.[48] found that hydrogen adsorption at ambient conditions can reach almost 0.6 wt% which is far too low to be useful for automotive applications. Wu et al.[49] have studied the influence of temperature, pressure and geometrical structure of pillared graphene on hydrogen adsorption; they concluded that the H_2 uptake of graphene is higher than that of carbon nanotubes and that low temperature, high pressures and larger interlayer distance between the graphene sheets maximize the hydrogen storage capacity.

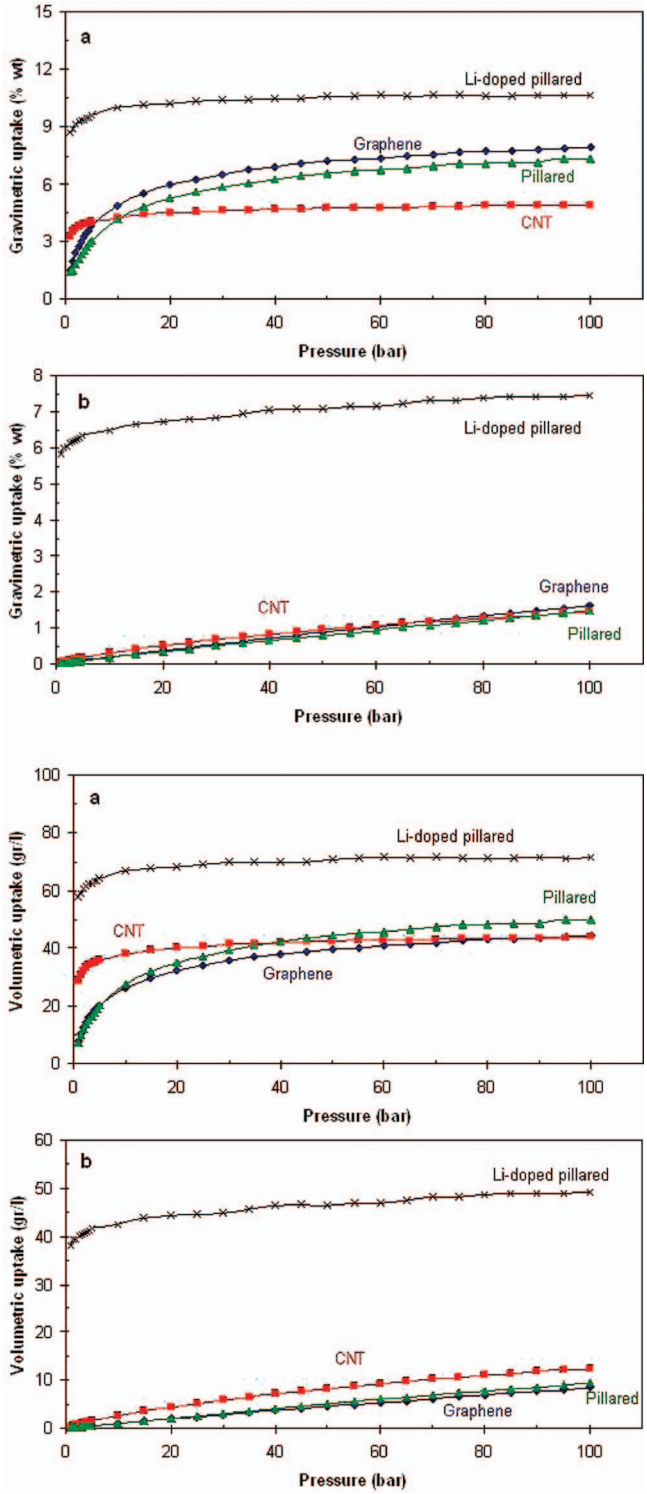

Figure 10. (upper) Gravimetric hydrogen uptake for graphene (diamonds), (6,6) carbon nanotubes (squares), pillared material (triangles), and Li-doped pillared material (stars) at (a) 77 K and (b) 300 K. [Reproduced with permission from Ref. 42] (below) Volumetric hydrogen uptake for graphene (diamonds), (6,6) carbon nanotubes (squares), pillared material (triangles), and Li-doped pillared (stars) at (a) 77 K and (b) 300 K. [Reproduced with permission from Ref. 42].

Doped/Decorated Graphene for Hydrogen Storage

An alternative approach to boost the adsorption capacity of hydrogen on graphene consists in suitably modifying the surface through

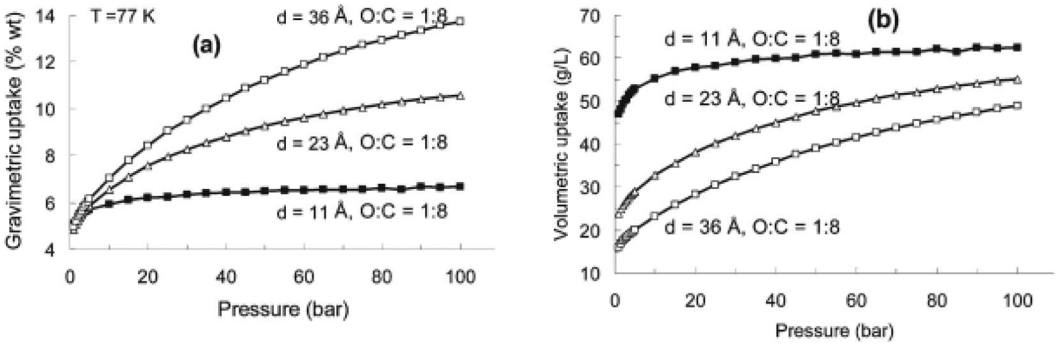

Figure 11. Gravimetric (a) and volumetric (b) H_2 adsorption isotherms of Li-doped pillared GO with doping ratio O/C = 1:8 for pore sizes (maximum distance between GO sheets or between pillars, depending which is bigger for a particular type of pore) d = 11, 23, and 36 Å. [Reproduced with permission from Ref. 44].

doping or adsorption of metals (alkali metals, alkaline earth metals, transition metals), as reported by many theoretical investigations. These studies indicate two pathways for enhanced hydrogen adsorption by interaction of H_2 molecules with metals. The first one relies on the polarization of H_2 by the electric field established by alkali metals leading to H_2 binding energies of approximately 0.2 eV,[50–54] these systems have been predicted to reach gravimetric capacities that not only meet D.O.E. targets but in most cases even surpass them. The use of an electric field to manipulate the hydrogen uptake by graphene was also discussed in the following papers of Ao et al.[55–57] The second approach exploits the so-called Kubas interactions,[58] i.e. it relies on hybridizing H_2 σ or σ* orbitals with transition metal electronic states to achieve binding energies between 0.2 and 0.6 eV and as a consequence potentially useful hydrogen storage capacities.[59–69]

Liu et al.[70] have applied this approach to Ti-decorated graphene; their density functional (DFT) calculations have predicted a high hydrogen storage capacity due to enhanced binding energies of molecular hydrogen with Ti atoms. The Ti atoms do not form clusters in this case, thus facilitating maximum hydrogen adsorption. For other transition metal clustering, which is favored by their large cohesive energy, can represent a significant obstacle to efficient H_2 adsorption.[71,72] In fact, clustering prevents dissociation and thereby decreases the hydrogen storage capacity. For that reason metals with smaller cohesive energy, such as alkali metals or alkaline earth metals have attracted much attention in this context.[73,74] Calcium with its cohesive energy of 1.8 eV meets this criterion[75,76] and Lee et al.[77] have proposed a system of graphene decorated with calcium, capable of adsorbing H_2 molecules with binding energies around 0.2 eV based on the hybridization of the unoccupied Ca 3d states with H_2 σ states and polarization of the H_2 molecules. These authors have suggested that isolated Ca atoms prefer to adsorb on the zigzag edges of graphene (Figure 13) leading to a gravimetric hydrogen storage capacity of 5 wt%. Similarly Beheshti et al.[78] have investigated the adsorption of hydrogen on calcium-decorated boron doped graphene using first principle calculations and found a gravimetric storage capacity of 8.32 wt%. An even larger hydrogen storage capacity (11.7 wt%) has been reported for Na-decorated boron doped graphene by Wang et al.[79] To the best of our knowledge, no experimental verification of these predictions is available so far.

Hydrogen storage capacities comparable to those of Ca-decorated graphene have been predicted by Ao et al.[80] for graphene doped with Al. These authors have performed ab initio molecular dynamics calculation to study the effects of temperature and pressure on the adsorption/desorption kinetics and found a maximum hydrogen gravimetric capacity of 5.13 wt% at 300 K and 0.1 Gpa. A much more spectacular result has been obtained by Ao and Peeters,[81] who found that a graphene layer decorated with Al on both sides can store hydrogen up

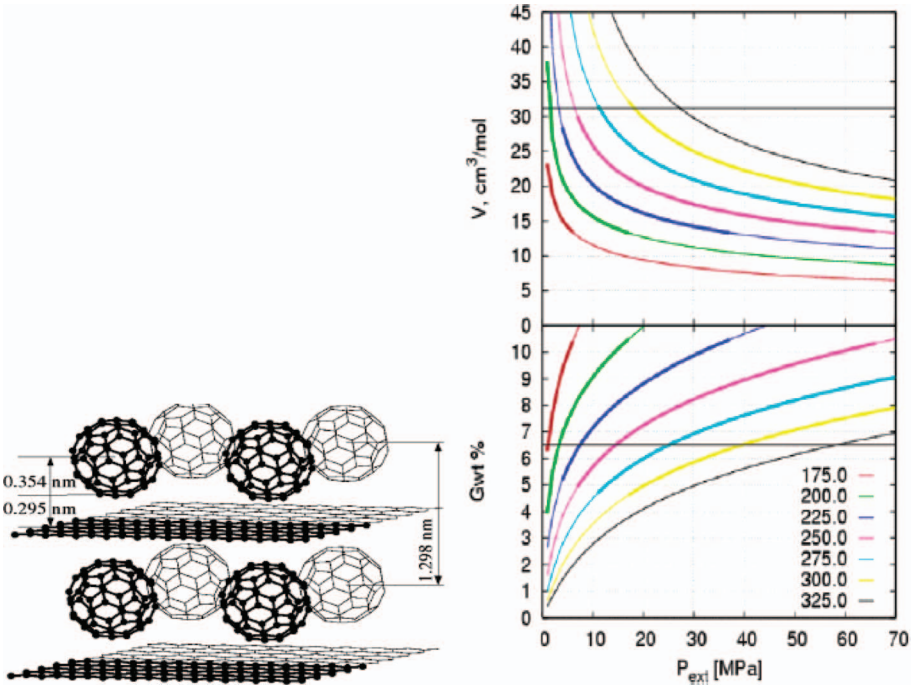

Figure 12. (left) The extended unit cell of C_{60}-intercalated graphite where the fullerene molecules form two-dimensional hexagonal layers. Volumetric (right top) and gravimetric storage (right down) capacities of C_{60}-intercalated graphite, calculated from the real gas equation of state, as function of the external pressure are given for various temperatures (color coded). The targets of the D. O.E. for automotive applications (gravimetric storage capacity = 6.5 wt%, volumetric storage capacity = 31.2 cm^3/mol) are indicated as horizontal lines. [Reproduced with permission from Ref. 46].

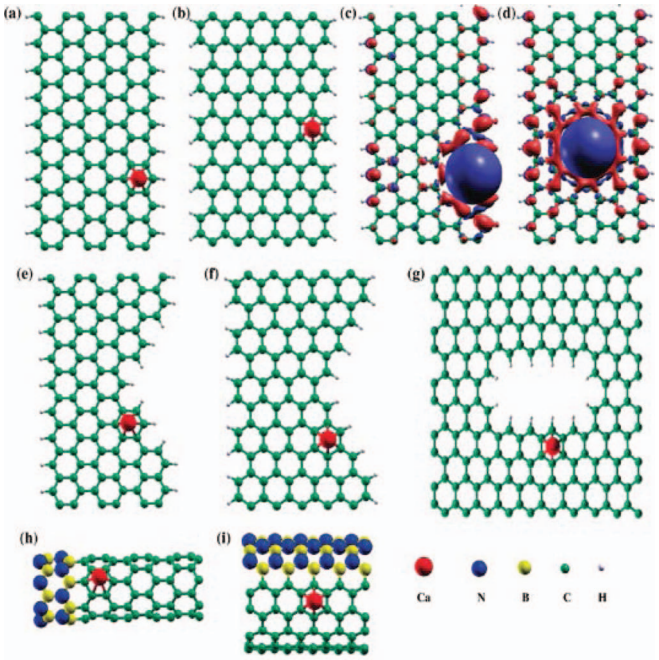

Figure 13. (a,b) The optimized atomic geometries for a Ca atom adsorbed on the edge of a zigzag and an armchair graphene nanoribbon, respectively. (c,d) The charge density difference between the Ca atom and the zigzag nanoribbon with the isosurface value of 0.0005 e/(au)^3 when the Ca atom is attached on the edge and in the middle, respectively. Red colors indicates electron accumulation and blue electron depletion. (e-i) The optimized atomic structures of a Ca atom adsorbed on the armchair edge of a zigzag-armchair-edged graphene nanoribbon, the zigzag edge of an armchair-zigzag-edged graphene nanoribbon, the zigzag edge of a large vacancy-defected graphene, a (7,0) C-BN nanotube junction, and a (7,7) mixed C-BN nanotube. [Reproduced with permission from Ref. 77].

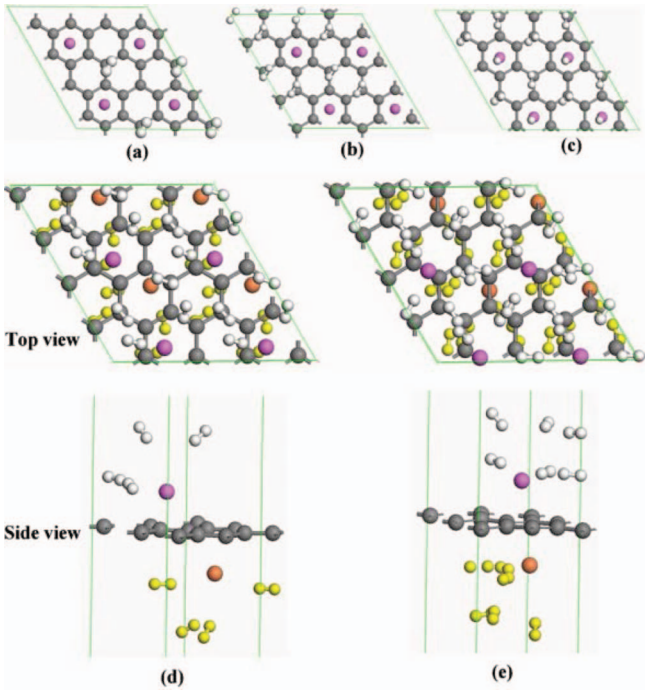

Figure 14. Atomic structures of H_2 molecules adsorbed on Al-decorated graphene. (a) One H_2 molecule adsorbed on graphene with Al adsorbed only on one side, (b) two H_2 molecules adsorbed on graphene with Al adsorbed only on one side of graphene, (c) three H_2 molecules adsorbed on graphene with Al adsorbed only on one side of graphene, (d) four H_2 molecules adsorbed on each side of graphene with Al adsorbed on both sides, and (e) six H_2 molecules adsorbed on each side of graphene with Al adsorbed on both sides. In this figure, $4 \times 4 \times 1$ supercells are plotted to better display the adsorption sites of the H_2 molecules. In (d) and (e), to evidence the Al atoms and H_2 molecules adsorbed on both sides of graphene, Al atoms and H_2 molecules below the graphene layer are shown as orange and yellow, respectively. Meanwhile, in order to show the two-layer adsorption arrangement of H_2 molecules, initial simulation cells of side view are also given in the nether part of (d) and (e). [Reproduced with permission from Ref. 81].

to 13.79 wt% with average adsorption energy −0.193 eV/H_2, which by far exceeds D.O.E. targets. This remarkable uptake of H_2 is due to the fact that the adsorbed Al atoms act as bridges that link the electron clouds of the H_2 molecules and the graphene layer. As illustrated in (Figure 14) this entails a two-layer arrangement of H_2 molecules on each side of the Al-decorated graphene layer.

Hydrogen Storage by the Spillover Process

Recently another mechanism for enhanced hydrogen adsorption on carbon nanostructures, known as the spillover process, has attracted much attention. This mechanism was first suggested in 1933[82] and again in 1964[83] for H_2 adsorption on carbon black are decorated with Pt and describes the adsorption process as a fast catalytically induced dissociation on the metal followed by slow hydrogen surface diffusion from the hydrogen-saturated metal catalyst to the carbon substrate.

Following up on this, Lueking and Yang[84,85] have reported that metal catalysts present on multi-walled carbon nanotubes are able to increase the adsorption capacity of H_2 to gravimetric values of 3.7 wt%. Li and Yang tested different types of carbon structures for spillover processes, namely activated carbons[86,87] metal-organic frameworks[88–90] and graphite nanofibers,[91] and demonstrated enhanced hydrogen adsorption at ambient conditions for all of them. However, despite these high hydrogen storage capacity values, the complete understanding of the mechanism as well as for the diffusion behavior of the hydrogen atoms and the way they chemisorb on the carbon substrate is still missing. For these reasons numerous studies of the spillover process on graphene have been carried out and the most important ones will be illustrated in the next paragraphs.

Psofogianakis and Froudakis[92] were the first to study the spillover mechanism of Pt_4 clusters on graphite (0001) by density functional theory. They confirmed that H_2 molecules dissociate readily on platinum clusters and found that the diffusion barrier for physisorbed hydrogen on graphite is very small, while it increases significantly for chemisorbed hydrogen. This means that the H atoms have to overcome a high energy barrier to migrate from the platinum cluster to the graphite substrate (Figure 15). If graphene is replaced with graphene oxide,[93] the barrier for migration from Pt_4 to GO has been found to be lower because the H atom can now migrate to an epoxide O on the surface; the same is true for the diffusion barrier of hydrogen on GO, allowing for free diffusion.

Going one step further by considering how B-doping affects hydrogen adsorption on graphene, Wu et al.[94] have determined that the adsorption strength for both H atoms and metal clusters on the doped substrate is enhanced and that a saturated Pt_4 binds 14 hydrogen, while the same cluster on pure graphene saturates with only 10 hydrogen atoms. Furthermore, the estimated activation barrier for one hydrogen atom migrating from the platinum cluster to B-doped graphene is much lower due to an enhanced C-H binding strength (Figures 16 and 17).

A big contribution to the understanding of the spillover process has been made by Yakobson group,[95] who first did not consider the catalyst *per se* but focused on the variation of the hydrogen binding to graphene and its thermodynamic comparison with gaseous H_2. Using ab initio methods they have shown that hydrogen forms clusters which are influenced by aromaticity rules and pyramidalization strain[96,97] and which are characterized by dramatically increased binding energies as compared to single hydrogen. The best binding configuration is found for islands with fully hydrogenated hexagons (Figures 18 and 19). The authors also predict that the hydrogen storage capability can

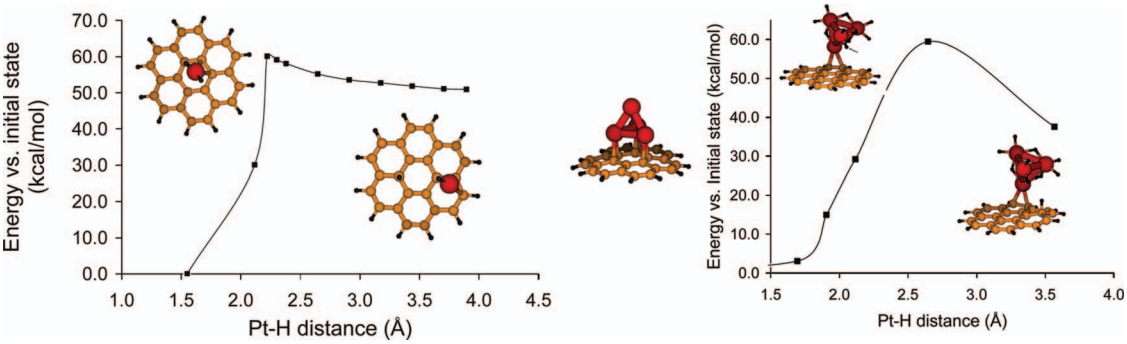

Figure 15. (left panel) Energy scan for the migration of a H atom from a Pt atom to the coronene surface. The energy is referenced to the initial state where both H atoms are adsorbed on the Pt atom. Inset: Initial and final structures for the migration. (right panel) Energy scan for the migration of a H atom from the fully saturated Pt_4 cluster to the coronene surface. Inset: initial and final structures for the migration. Left of the graph: Pt_4 cluster on coronene. The line connecting the points in both graphs is a guide to the eye. [Reproduced with permission from Ref. 92].

reach 7.7 wt% and that the balance between the fluidic gas phase and the immobilized "storage" phase can be changed in either direction by tuning pressure and temperature not too far from the ambient conditions, a condition which is highly desirable for efficient loading/unloading in practical applications. These findings agree with the report of graphane, the fully hydrogenated form of graphene, by Elias et al.[98] readily obtained by exposing graphene to a cold hydrogen plasma and its backconversion to graphene by annealing to 450°C in an Ar atmosphere. However, while the original paper[98] states a very good stability of graphane in ambient conditions, a recent review paper also of the Manchester group reports[99] that graphene gradually loses its hydrogen but whether this is a problem for hydrogen storage applications remains to be investigated.

After having considered H binding to graphene, the Yakobson group extended their work to small Ni and Pd clusters on graphene and on hydrogenated graphene and demonstrated the thermodynamic and kinetic plausibility of the spillover process.[100] Their main findings can be summarized as follows: from the energetic point of view, spillover of hydrogen is unfavorable for pristine graphene but can occur even before the metal cluster saturates on the hydrogenated graphene surface, where it strengthens C-H bonding. The calculated energy barriers for the H migration from the metal cluster to the substrate have been found to be compatible with spillover even below room temperature. Most importantly for future developments, along with the catalyst saturation, the optimum C-H bonding has emerged as a decisive factor for realizing the spillover. Therefore, any modification of hydrogenated graphene such as incorporation of defects, curvature, and dopants that lead to an increased C-H bonding will also amplify the spillover. So far no experimental has been reported that verifies these predictions.

Also alkaline earth metal-decorated graphene was examined for the possibility of realizing the spillover effect. Gao et al.[101] have found with first principle total energy calculations that adsorption of the first H_2 on single Ca atoms on graphene is dissociative but also enhances the system stability. Thus further adsorption of hydrogen molecules on Ca-decorated graphene is weak and not promising for hydrogen storage applications. However, if graphene is decorated with Ca dimers, evidence for spillover was found; in fact, when two H_2 atoms adsorbed dissociatively on a Ca dimer, one of the four H chemisorbs on graphene more stably by 0.37 eV than on the Ca dimer. If the hydrogen coverage was increased, just as discussed above for pristine graphene,

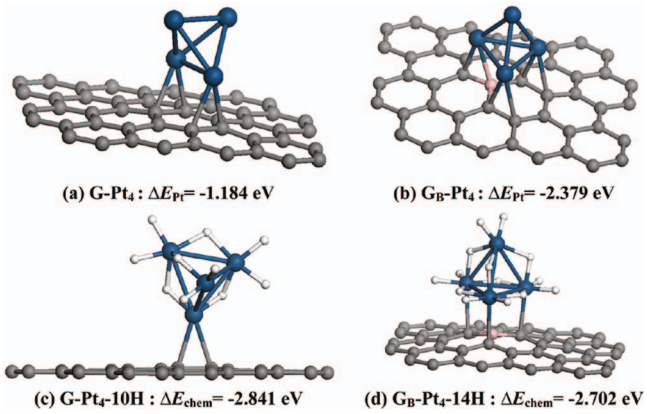

Figure 16. Optimized structures of (a) a Pt_4 cluster on pure graphene (G-Pt_4), (b) a Pt_4 cluster on a boron-doped graphene sheet (GB -Pt_4), (c) a saturated Pt_4 cluster on graphene with 10 chemisorbed H atoms (G-Pt_4-10H), and (d) a saturated Pt_4 cluster on boron-doped graphene with 14 chemisorbed H atoms (GB-Pt_4-14H). The binding strength of Pt_4, $|\Delta E_{Pt}|$, on boron-doped graphene is 2.379 eV, much stronger than that of 1.184 eV on pure graphene. The chemisorption energy per H atom ΔE_{chem} for the saturated Pt_4 cluster on pure and B-doped graphene is -2.841 and -2.702 eV, respectively, indicating a strong H_2 dissociation ability for the metal cluster. [Reproduced with permission from Ref. 94].

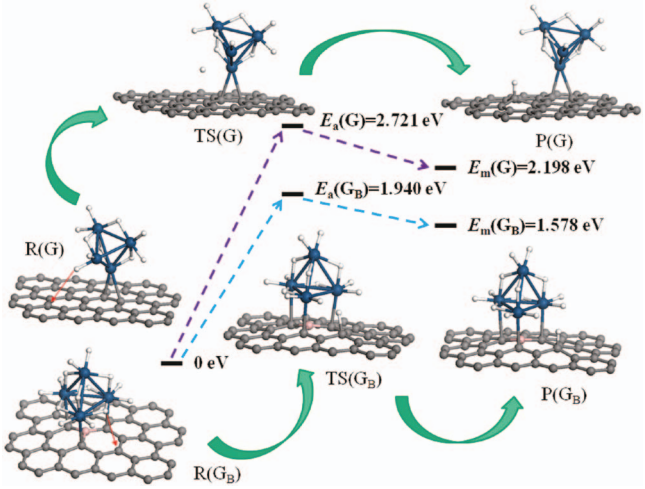

Figure 17. Optimized structures of initial (R), transition (TS), and final (P) states for the H migration process from a saturated Pt_4 cluster to the supporting graphene or B-doped graphene substrate. The black bars denote the relative energy levels of these structures, with the corresponding schematic diagrams (H, white; B, pink; C, gray; Pt, blue) drawn above or below. The calculated activation energy, E_a, for H migration from Pt_4 to graphene is 2.721 eV and from Pt_4 to B-doped graphene 1.940 eV. The purple and blue dashed arrows are respectively used to guide the eye for the two separate migration paths on graphene and B-doped graphene. The reaction energy of the migration, E_m, with respect to the initial state is estimated to be 2.198 eV and 1.578 eV, respectively, for graphene and B-doped graphene. [Reproduced with permission from Ref. 94].

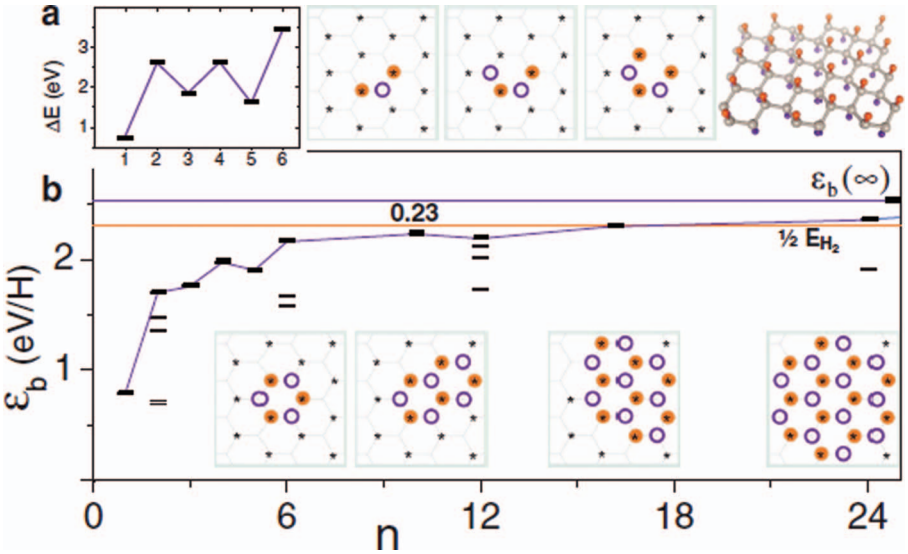

Figure 18. The aromaticity effect and closed six-ring preference for H chemisorbed on graphene. The energy increment ΔEn due to nth atom sorption versus its number (a). In (b), binding energy per H for all clusters considered as a function of their size n. Illustrating some energy points, the insets show 3, 4, and 5 adsorbed H atoms, followed by the larger closed-ring structures with 6, 10, 16, and 24 atoms, and the infinite fully hydrogenated graphene. In (b), the thin line connects the most stable configurations to guide the eye. [Reproduced with permission from Ref. 95].

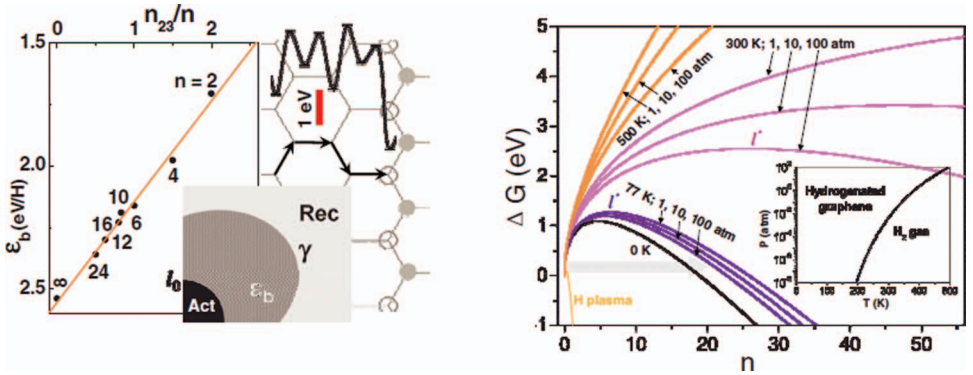

Figure 19. (left) The computed energies of hydrogen binding into compact aromatic clusters (with bound H atoms alternating at both sides of the graphene) depend linearly on the portion $n23/n$ of sp^2-sp^3 bonds. The inset schematics show an activator-catalyst (black) next to the island of hydrogenated graphene (dark gray) on the receptor. Energies of H atom and the diffusion barriers several steps near the interface are shown on the right side. (right) Gibbs free energy of formation of a CH island in the graphene as a function of number of H, computed for different pressure (P) and temperature (T). The typical nucleation-type shapes are characterized by the critical nucleus size (number of atoms, n^*, or dimension l^*) and the nucleation barrier. The nearly vertical thin downward line corresponds to the atomic plasma, where the chemical potential is high and the nucleation barrier vanishes. The horizontal gray arrow indicates a possible role of the catalyst particle as a nucleation seed. The inset shows thermodynamic equilibrium line between the H_2 gas and the storage phase (CH). [Reproduced with permission from Ref. 95].

the binding energy of hydrogen atoms also increased. The hydrogen storage capacity via the spillover mechanism in Ca-adsorbed graphene has been found to depend on Ca coverage and to reach 7.7 wt %.

Conclusions

Hydrogen is expected to play a major role as future "green" fuel for mobility and transport applications but the big challenge of finding a material capable of storing very high amounts of H_2, at ambient conditions as to make this fuel also economically viable has still to be overcome. Theoretical simulations of hydrogen adsorption on graphene and graphene oxide are very promising and approach D.O.E. targets. Even higher hydrogen storage capacities are predicted for graphene and graphane decorated with transition metal clusters or alkali/alkaline earth metals. However, concerning experimental results only the adsorption of hydrogen on graphene has been studied so far and a gravimetric storage capacity of 4 wt% was found while all the other much more competitive predictions still await experimental confirmation.

References

1. The Department of Energy (DOE), Office of Energy Efficiency and Renewable Energy's Fuel Cell Technologies Program: Hydrogen Storage. http://www.eere.energy.gov/hydrogenandfuelcells/storage/ (2009).
2. S. Satyapal, J. Petrovic, C. Read, G. Thomas, and G. Ordaz, *Catal. Today*, **120**, 246 (2007).
3. J. Arthur, J. Esswein, and Daniel G. Nocera, *Chem. Rev.*, **107**, 4022 (2007).
4. L. Schlapbach and A. Züttel, *Nature*, **414**, 353 (2001).
5. R. Strobel, J. Garche, P. T. Moseley, P. L. Jorissen, and G. J. Wolf, *Power Sources*, **159**, 781 (2006).
6. N. L. Rosi, J. Eckert, M. Eddaoudi, D. T. Vodak, J. Kim, M. O'Keeffe, and O. M. Yaghi, *Science*, **300**, 1127 (2003).
7. J. L. C. Rowsell and O. M. Yaghi, *Angew. Chem., Int. Ed.*, **44**, 4670 (2005).
8. A. C. Dillon, K. M. Johns, T. A. Bekkedahl, C. H. Kiang, D. S. Bethune, and M. J. Heben, *Nature*, **386**, 377 (1997).
9. A. Chambers, C. Park, R. T. K. Baker, and N. M. Rodriguez, *J. Phys. Chem. B*, **102**, 4253 (1998).
10. B. Panella, M. Hirscher, and S. Roth, *Carbon*, **43**, 2209 (2005).
11. Y. Yurum, A. Taral, and T. N. Veziroglu, *Int. J. Hydrogen Energy*, **34**, 3784 (2009).
12. D. Zhao, D. Yuan, and H.-C. Zhou, *Energy Environ. Sci.*, **1**, 222 (2008).
13. A. B. Bourlinos, Th. A. Steriotis, M. Karakassides, Y. Sanakis, V. Tzitzios, C. Trapalis, E. Kouvelos, and A. Stubos, *Carbon*, **45**, 852-7 (2007).

14. D.O.E. Office of Energy Efficiency and Renewable Energy Hydrogen, Fuel cells & infrastructure technologies program multi-year research, development and demonstration plan. Available from: www.eere.energy.gov/hydrogenandfuelcells/mypp.
15. K. S. Novoselov, A. K. Geim, S. V. Morozov, D. Jiang, Y. Zhang, S. V. Dubonos, I. V. Grigorieva, and A. A. Firson, *Science*, **306**, 666 (2004).
16. N. Castro, F. Guinea, N. M. R. Peres, K. S. Novoselov, and A. K. Geim, *Rev. Mod. Phys.*, **81**, 109 (2009).
17. C. Lee, X. Wei, J. W. Kysar, and J. Hone, *Science*, **321**, 385 (2008).
18. A. A. Balandin, S. Ghosh, W. Bao, I. Calizo, D. Teweldebrhan, F. Miao, and C. N. Lau, *Nano Lett.*, **8**, 902 (2008).
19. R. R. Nair, P. Blake, A. N. Grigorenko, K. J. Booth, T. Stauber, N. M. R. Peres, and A. K. Geim, *Science*, **320**, 1308 (2008).
20. M. D. Stoller, S. Park, Y. Zhu, J. An, and R. S. Ruoff, *Nano Lett.*, **8**, 3498 (2008).
21. A. Züttel, P. Sudan, P. Mauron, T. Kiyobayashi, C. Emmenegger, and L. Schlapbach, *Int J Hydrogen Energy*, **27**, 203 (2002).
22. V. Tozzini and V. Pellegrini, *Phys. Chem. Chem. Phys.*, **15**, 80 (2013).
23. S. Patchkovskii, S. J. Tse, N. S. Yurchenko, L. Zhechov, T. Heine, and G. Seifert, *PNAS*, **102**, 10439 (2005).
24. J. S. Arellano, L. M. Molina, and A. Rubio, *J. Chem. Phys.*, **112**, 8114 (2000).
25. F. Dakrim, J. Vermesse, P. Malbrunot, and D. Levesque, *J. Chem. Phys.*, **110**, 4020 (1999).
26. F. Tran, J. Weber, T. A. Wesolowski, F. Cheikh, Y. Ellinger, and F. Pauzat, *J. Phys. Chem. B*, **106**, 8689 (2002).
27. T. Heine, L. Zhechkov, and G. Seifert, *Phys. Chem. Chem. Phys.*, **6**, 980 (2004).
28. V. Tozzini and V. Pellegrini *J. Phys. Chem. C*, **115**, 25523 (2011).
29. S. Goler, C. Colleti, V. Tozzini, V. Piazza, T. Mashoff, F. Beltram, V. Pellegrini, and S. Heun, *J. Phys. Chem. C*, **117**, 11506 (2013).
30. R. D. Dreyer, S. Park, W. C. Bielawski, and S. R. Ruoff, *Chem. Soc. Rev.*, **39**, 228 (2010).
31. L. Wang, K. Lee, Y. Y. Sun, M. Lucking, Z. Chen, J. J. Zhao, and B. S. Zhang, *ACS Nano*, **3**, 2995 (2009).
32. W. J. Burress, S. Gadipelli, J. Ford, M. J. Simmons, W. Zhou, and T. Yildirim, *Angew. Chem. Int. Ed.*, **49**, 8902 (2010).
33. K. S. Subrahmanyam, P. Kumar, U. Maitra, A. Govindaraj, K. P. S. S. Hembram, U. V. Waghmare, and C. N. R. Rao, *PNAS*, **108**, 2674 (2011).
34. K. S. Subrahmanyam, S. R. C. Vivekchand, A. Govindaraj, and C. N. R. Rao, *J. Mater. Chem.*, **18**, 1517 (2008).
35. K. S. Subrahmanyam, L. S. Panchakaria, A. Govindaraj, and C. N. R. Rao, *J. Phys. Chem. C*, **113**, 4257 (2009).
36. A. J. Birch, *J. Chem. Soc.*, 430 (1944).
37. A. Govindaraj, *Curr. Sci. India*, **65**, 868 (1993).
38. Z. Jin, W. Lu, K. J. O'Neill, P. A. Parilla, L. J. Simpson, C. Kittrell, and J. M. Tour, *Chem. Mater.*, **23**, 923 (2011).
39. G. Srinivas, Y. Zhu, R. Piner, N. Skipper, M. Ellerby, and R. Ruoff, *Carbon*, **48**, 630 (2010).
40. S. H. Aboutalebi, S. Aminorroaya-Yamini, I. Nevirkovets, K. Konstantinov, and H. K. Liu, *Adv. Energy Mater.*, **2**, 1439 (2012).
41. C. X. Guo, Y. Wang, and C. M. Li, *ACS Sustainable Chem. Eng.*, **1**, 14 (2013).
42. G. K. Dimitrakakis, E. Tylianakis,and, and G. E. Froudakis, *Nano Lett.*, **8**, 3166 (2008).
43. M. Bendikov, F. Wudl, and D. F. Peperichka, *Chem. Rev.*, **104**, 4891 (2004).
44. E. Tylianakis, G. M. Psofogiannakis, and G. E. Froudakis, *J. Phys. Chem. Lett.*, **1**, 2459 (2010).
45. E. Tylianakis, E. Klontzas, and G. E. Froudakis, *Nanotechnology*, **20**, 204030/1 (2009).
46. A. Kuc, L. Zhechov, S. Patchkovskii, G. Seifert, and T. Heine, *Nano Lett.*, **7**, 1 (2007).
47. Y. N. R. Gengler, D. Gournis, A. H. Aimon, L. M. Toma, and Petra Rudolf, *Chem.-Eur. J.*, **18**, 7594 (2012).
48. Y. Matsuo, S. Ueda, K. Konioshi, J. P. Marco-Lozar, D. Lozano-Castello, and D. Amoros-Cazorla, *Int. Journal of Hydrogen Energy*, **37**, 10702 (2012).
49. C.-D. Wu, T.-H. Fang, and J.-Y. Lo, *Int. J. Hydrogen Ener.*, **37**, 14211 (2012).
50. Q. Sun, P. Jena, Q. Wang, and M. Marguez, *J. Am. Chem. Soc.*, **128**, 9741 (2006).
51. K. R. S. Chandrakumar and S. K. Ghosh, *Nano Lett.*, **8**, 13 (2008).
52. M. Yoon, S. Yang, C. Hicke, E. Wang, D. Geohegan, and Z. Zhang, *Phys. Rev. Lett.*, **100**, 206806 (2008).
53. Q. Wang, Q. Sun, P. Jena, and Y. Kawazoe, *J. Chem. Theory Comput.*, **5**, 374 (2009).
54. M. Yoon, S. Yang, E. Wang, and Z. Zhang, *Nano Lett.*, **7**, 2578 (2007).
55. Z. M. Ao and S. Li, *J. Phys. Chem. C*, **114**, 14503.
56. Z. M. Ao and F. M. Peeters, *Appl. Phys. Lett.*, **96**, 253106 (2010).
57. Z. M. Ao, A. D. Hernández-Nieves, F. M. Peeters, and S. Li, *Phys. Chem. Chem. Phys.*, **14**, 1463 (2012)
58. G.J Kubas, *J. Organomet. Chem.*, **635**, 37 (2001).
59. Y. Zhao, Y.-H. Kim, A. C. Dillon, M. J. Heben, and S. B. Zhang, *Phys. Rev. Lett.*, **94**, 155504 (2005).
60. T. Yildirim and S. Ciraci, *Phys. Rev. Lett.*, **94**, 175501 (2005).
61. W. H. Shin, S. H. Yang, W. A. Goddard, and J. K. Kang, *Appl. Phys. Lett.*, **88**, 053111 (2006).
62. H. Lee, W. I. Choi, and J. Ihm, *Phys. Rev. Lett.*, **97**, 056104 (2006).
63. E. Durgun, S. Ciraci, W. Zhou, and T. Yildirim, *Phys. Rev. Lett.*, **97**, 226102 (2006).
64. S. Meng, E. Kaxiras, and Z. Zhang, *Nano Lett.*, **7**, 663 (2007).
65. N. Park, S. Hong, G. Kim, and S.-H. Jhi, *J. Am. Chem. Soc.*, **129**, 8999 (2007).
66. Y. Zhang, N. W. Franklin, R. J. Chen, and H. J. Dai, *Chem Phys Lett.*, **331**, 35 (2000).
67. E. Durgun, S. Ciraci, and T. Yildirim, *Phys Rev B*, **77**, 085405 (2008).
68. T. Yildirim and S. Ciraci, *Phys. Rev. Lett.*, **94**, 175501 (2005).
69. Y. Zhao, Y.-H. Kim, A. C. Dillon, M. J. Heben, and S. B. Zhang, *Phys. Rev. Lett.*, **94**, 155504 (2005).
70. Y. Liu, L. Ren, Y. He, and H. P. Cheng, *J. Phys. Condens. Matter.*, **22**, 445301 (2010).
71. Q. Sun, Q. Wang, P. Jena, and Y. Kawazoe, *J. Am. Chem. Soc.*, **127**, 14582 (2005).
72. S. Li and P. Jenaq, *Phys. Rev. Lett.*, **97**, 209601 (2006).
73. P. Chen, X. Wu, J. Lin, and K. L. Tan, *Science*, **285**, 91 (1999).
74. R. T. Yang, *Carbon*, **38**, 623 (2000).
75. C. Ataca, E. Akturk, and S. Ciraci, *Phys. Rev. B*, **79**, 041406 (2009).
76. W. Kohn and L. J. Sham, *Phys. Rev.*, **140**, 1133 (1965).
77. H. Lee, J. Ihm, M. L. Cohen, and S. G. Louie, *Nano Lett.*, **10**, 793 (2010).
78. E. Beheshti, A. Nojeh, and P. Servati, *Carbon*, **49**, 1561 (2011).
79. F. D. Wang, F. Wang, N. N. Zhang, Y. H. Li, S. W. H. Sun, Y. F. Chang, and R. S. Wang, *Chem. Phys. Lett.*, **555**, 212 (2013).
80. Z. M. Ao, Q. Jiang, R. Q. Zhang, T. T. Tan, and S. Li, *J. Appl. Phys.*, **105**, 074307 (2009).
81. Z. M. Ao and F. M. Peeters, *Phys. Rev. B*, **81**, 205406 (2010).
82. R. K. Burstein, P. Lewin, and S. Petrow, *Physik. Z.*, **4**, 197 (1933).
83. A. J. Robell, E. V. Ballou, and M. Boudart, *J. Phys. Chem.*, **68**, 2748 (1964).
84. A. Lueking and R. T. Yang, *J. Catal.*, **206**, 165 (2002).
85. A. Lueking and R. T. Yang, *AIChE J.*, **49**, 1556 (2003).
86. A. J. Lachawiec, G. S. Qi, and R. T. Yang, *Langmuir*, **21**, 11418 (2005).
87. A. Lueking and R. T. Yang, *Appl. Catal.* A, **265**, 259 (2004).
88. Y. W. Li and R. T Yang, *J. Am. Chem. Soc.*, **128**, 726 (2006).
89. Y. W. Li and R. T. Yang, *J. Am. Chem. Soc.*, **128**, 8136 (2006).
90. Y. W. Li and R. T. Yang, *AIChE J.*, **54**, 269 (2008).
91. A. D. Lueking and R. T. Yang, *Appl. Catal. A*, **265**, 259 (2004).
92. G. M. Psofogiannakis and G. E. Froudakis, *J. Phys. Chem. C.*, **113**, 14908 (2009).
93. G. M. Psofogiannakis and G. E. Froudakis, *J. Am. Chem. Soc.*, **131**, 15133 (2009).
94. H.-Y. Wu, X. Fan, J.-L. Kuo, and W.-Q. Deng, *J. Phys. Chem. C*, **115**, 9241 (2011).
95. Y. Lin, F. Ding, and B. I. Yakobson, *Phys. Rev. B*, **78**, 041402 (2008).
96. R. C. Haddon, *J. Phys. Chem.*, **91**, 3719 (1987).
97. R. C. Haddon, *Science*, **261**, 1545 (1993).
98. D. C. Elias, R. R. Nair, T. M. G Mohiuddin, S. V. Morozov, P. Blake, M. P. Halsall, A. C. Ferrari, D. W. Boukhvalov, M. I. Katsnelson, A. K. Geim, and K. S. Novoselov, *Science*, **323**, 610 (2009).
99. A. K. Geim and I. V. Grigorieva, *Nature*, **499**, 419 (2013).
100. A. K. Singh, M. A. Ribas, and B. I. Yakobson, *ACS Nano*, **3**, 1657 (2009).
101. Y. Gao, N. Zhao, L. Jiajun, H. Chunnian, and S. Chunsheng, *J. Hydrogen Energy*, **37**, 11835 (2012).